Davydov soliton dynamics: two-quantum states and diagonal disorder

1991 J. Phys.: Condens. Matter 3 3235

(http://iopscience.iop.org/0953-8984/3/19/003)

J. Phys.: Condens. Matter 3 (1991) 3235–3254. Printed in the UK

Davydov soliton dynamics: two-quantum states and diagonal disorder

Wolfgang Förner

Department of Theoretical Chemistry, Laboratory of the National Foundation for Cancer Research, Friedrich-Alexander-University Erlangen-Nürnberg, Egerlandstrasse 3, D-8520 Erlangen, Federal Republic of Germany

Received 2 August 1990, in final form 10 December 1990

Abstract. Our investigation of the dynamics of two-quantum states within Davydov $|D_2\rangle$ dynamics reveals remarkable differences from one-quantum dynamics. Soliton formation and pinning starts from smaller values of the non-linearity parameter X. From $X = 30$ pN propagating solitons from $X = 62$ pN pinned solitons are observed if both quanta are on the same end of the chain in the initial state. In the case of soliton collisions, the solitons penetrate each other unperturbed for small X, but fuse to a pinned two-quantum soliton for large X. Both one- and two-quantum states are very sensitive to diagonal disorder in the Hamiltonian. In $|D_1\rangle$ *ansatz* states, the soliton is found to appear for larger non-linearity but its sensitivity to diagonal disorder is essentially unchanged.

1. Introduction

Since their discovery, solitons have been used for the explanation of a wide variety of physical and chemical phenomena. Solitary solutions, i.e. non-dispersive or slowly dispersive wavepackets, can occur only in systems with non-linear forces. The importance of such non-linear forces is obvious, e.g. from the fact that a harmonic lattice would have an infinite heat conductivity [1]. The first observation of a solitary wavepacket in water was reported by Scott-Russel [2]. Some examples of the applications of soliton concepts are the dynamics of ferro- and antiferromagnetic materials [3, 4], rotation around carbon–carbon bonds in polyethylene [5], phase changes in solids [6, 7], the dynamics of the sugar–phosphate backbone [8] or the nucleotide bases [9, 10] in deoxyribonucleic acid (DNA) and the spin-less charge transport in *trans*-polyacetylene [11].

An important biological problem is the mechanism of energy transfer and storage in proteins [12]. Following Davydov's idea [13], one can assume that energy from adenosine triphosphate (ATP) hydrolysis is stored in the C=O stretching mode (amide I) of a polypeptide chain. Owing to the coupling of the mode to acoustic phonons in the lattice, non-linear forces appear, which can localize the excitation. Because of the coupling between the amide-I oscillators, this localized wavepacket is able to propagate [13] as a solitary wave. Since the complex structure of proteins makes measurements quite difficult, direct experimental evidence for the existence of such solitons is missing. However, in acetanilide (*N*-phenylacetamide) crystals, a new band appearing in low-temperature infrared and Raman spectra could only be explained by a model similar to

0953-8984/91/193235 + 20 $03.50

the concept of Davydov solitons but involving coupling to optical phonons [14]. However, there is evidence that the soliton in acetanilide is pinned.

Therefore, in proteins up to now one has had to perform computer experiments on the Davydov solitons, incorporating as many details of the physical nature of proteins as possible. These computer experiments can answer the question whether or not the proposed mechanism can function under 'realistic' conditions. Two very important aspects of the real situation that need to be incorporated into the model are the aperiodicity of proteins (20 different natural amino acids exist) and temperature ($\simeq 300$ K). In a preceding paper we have reported our study on aperiodicity effects on Davydov solitons [15]. We found the soliton to be stable over a rather wide range of aperiodicity in the parameters of the model Hamiltonian. However, the important effects of diagonal disorder have, at least to our knowledge, not been studied up to now. Therefore, in this paper, we report on our work concerning diagonal disorder in the model Hamiltonian. Since ATP hydrolysis provides approximately twice the energy of an amide-I quantum [16], we also study the dynamics of two-quantum states in some detail. To our knowledge, there exists no detailed investigation on the parameter dependence of the dynamics of two-quantum states, besides the study by Scott [16], where the norm of the state takes the value 2. In our study we use the newly derived [17] equations of motion for several-quantum states. These equations have been applied, to our knowledge, only in simulations at $T = 300$ K for special parameter values [18]. Soliton collisions have been studied by Bolterauer [19], but also only for one set of parameter values. Our results on temperature effects on soliton dynamics, which are more detailed than in our previous paper [15, 20], will be published elsewhere [21]. In that paper we will also compare in detail our results with those of other models for the inclusion of temperature [18, 22–29].

2. Method

The Hamiltonian used for this study is of the simple form suggested by Davydov [13] but extended to allow for diagonal disorder (the inclusion of disorder in all parameters is reviewed in the appendix):

$$\hat{H} = \sum_n [(E_0 + E_n)\hat{a}_n^+ \hat{a}_n - J(\hat{a}_n^+ \hat{a}_{n+1} + \hat{a}_{n+1}^+ \hat{a}_n) + \hat{p}_n^2/2M + \tfrac{1}{2}W(\hat{q}_n - \hat{q}_{n-1})^2 + X\hat{a}_n^+ \hat{a}_n(\hat{q}_n - \hat{q}_{n-1})]. \quad (1)$$

Note that, in contrast to most applications in the literature, we use the asymmetric interaction form of the Hamiltonian since the excitation energy of an amide-I oscillator is influenced far more by the hydrogen bond in which the C=O group participates than by the neighbouring one. Thus we use the term $X\hat{a}_n^+ \hat{a}_n(\hat{q}_n - \hat{q}_{n-1})$ instead of $X\hat{a}_n^+ \hat{a}_n(\hat{q}_{n+1} - \hat{q}_{n-1})$ as the oscillator–lattice coupling. More sophisticated forms of $\hat{H}$, incorporating more details of the protein structure, lead to the same qualitative results [30].

In equation (1), $\hat{a}_n^+$ ($\hat{a}_n$) are the usual boson creation (annihilation) operators [31] for the amide-I oscillators at sites n (see figure 1). The energy of an isolated vibrational quantum (CO stretch) can be deduced from infrared spectra ($E_0 = 0.205$ eV) [32]. E_n represents the diagonal disorder due to different amino acid side groups and local geometric distortions due to these groups in proteins. The dipole–dipole coupling

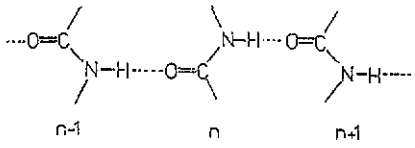

Figure 1. Schematic picture of a hydrogen-bonded channel in a protein.

between neighbouring amide-I oscillators is $J = 0.967$ meV [32]. The spring constant of the hydrogen bonds is usually assumed to be $W = 13\,\mathrm{N\,m^{-1}}$, a value measured in crystalline formamide [33]. However, since the peptide units in proteins are covalently bound in the backbone perpendicular to the spines (see figure 1), we expect W to be considerably larger than in formamide, where free molecules are vibrating [15]. Also in equation (1), $\hat{p}_n$ is the momentum and $\hat{q}_n$ the position operator of unit n. The average mass M is taken as that of myosin ($114m_p$) [32]. The energy of the CO stretching vibration in CO---HN hydrogen bonds is a function of the length r of the hydrogen bond ($E = E_0 + Xr$) [34]. The experimental value for X is 62 pN [32]. *Ab initio* Hartree–Fock calculations on formamide dimers usually lead to $X = 30$–50 pN [35, 36]. However, one has to keep in mind that the experimental value of X was obtained from the amide-I energies in crystals of materials containing CO---HN hydrogen bridges of different lengths. Thus the effects of the different side groups on the amide-I energy are probably also implicitly included in this value and not just the effect of the different hydrogen bond lengths.

For the solution of the time-dependent Schrödinger equation

$$\hat{H}|\psi\rangle = \mathrm{i}\hbar\frac{\partial}{\partial t}|\psi\rangle \tag{2}$$

we use the displaced oscillator state *ansatz* of Davydov [13] extended to states containing Q quanta [17]:

$$|\psi\rangle = \frac{1}{(Q!)^{1/2}}\left(\sum_n a_n'(t)\hat{a}_n^+\right)^Q \exp[-\hat{S}(t)]\,|0\rangle \tag{3a}$$

$$\hat{S}(t) = \frac{\mathrm{i}}{\hbar}\sum_m [\hat{p}_m q_m(t) - \hat{q}_m p_m(t)]. \tag{3b}$$

In this *ansatz*, $q_m(t)$ is the expectation value of the position operator and $p_m(t)$ that of the momentum operator of unit m, $|0\rangle$ is the vacuum state and $|a_n'(t)|^2$ is the probability of finding Q amide-I vibrational quanta at site n, provided that $\Sigma_n|a_n'|^2 = 1$.

In this so-called $|D_2\rangle$ *ansatz*, no phase mixing ('dressing') between phonons and excitons occurs. From (3), equations of motion can be obtained either by quantum-mechanical methods (QM) [17, 37] or by using the expectation value of $\hat{H}$ in state (3) as the classical Hamiltonian function (HM) [13, 30]. In Davydov's more sophisticated $|D_1\rangle$ *ansatz* [13], full phase mixing between excitations and phonons occurs. However, using this *ansatz* HM results in equations different from those obtained using the time-dependent variational principle [38] or other quantum-mechanical methods [39].

In their recent work Brown *et al* [40–42] have shown that, in the transportless case ($J = 0$), *ansatz* (3) leads to the correct time evolution of $q_n(t)$ but to an incorrect phonon energy. Note that for $J = 0$ the time-dependent Schrödinger equation can be solved exactly [40]. In case of the $|D_1\rangle$ *ansatz* [13] together with the equations of motion resulting

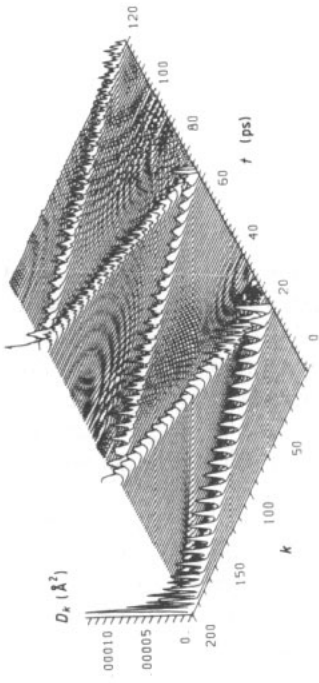
D_k (Å^2)
.00010
.00005
0
200
150
100
50
k
0
20
40
60
80
100
120
t (ps)

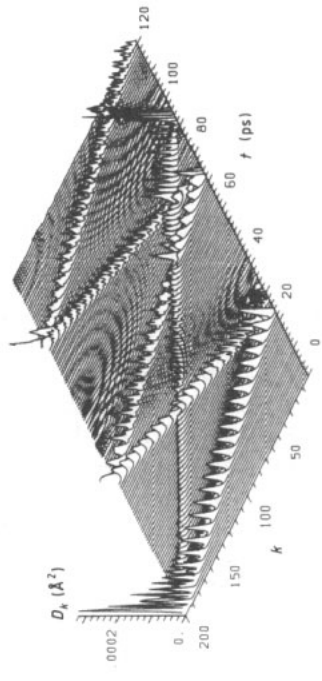
D_k (Å^2)
.0002
0
200
150
100
50
k
0
20
40
60
80
100
120
t (ps)

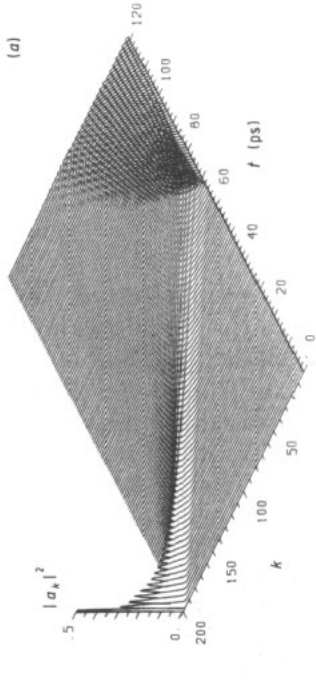
(a)
$|a_k|^2$
.5
0
200
150
100
50
k
0
20
40
60
80
100
120
t (ps)

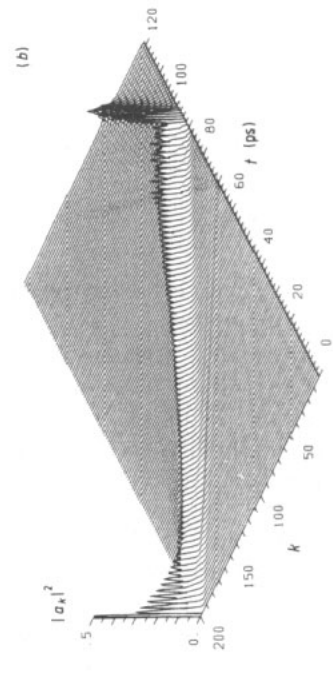
(b)
$|a_k|^2$
.5
0
200
150
100
50
k
0
20
40
60
80
100
120
t (ps)

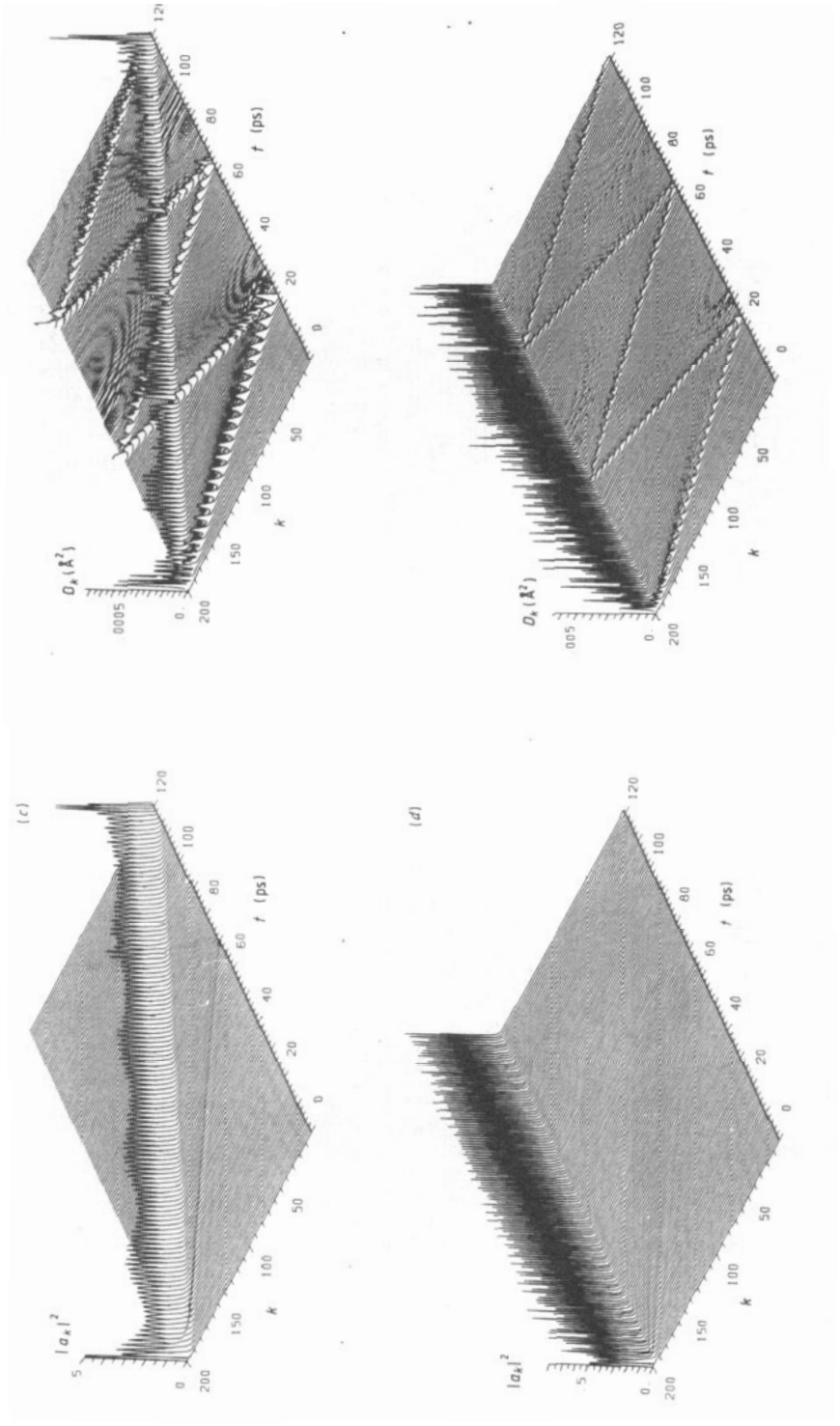

Figure 2. Time (t/ps) evolution of $|a_k(t)|^2$ and of the local lattice distortion $D_k = (q_k - q_{k-1})^2$ (Å^2) of a two-quantum state after initial excitation at the terminal site 199 and 198 as a function of X: (*a*) $X = 20$ pN; (*b*) $X = 31$ pN; (*c*) $X = 40$ pN; (*d*) $X = 62$ pN.

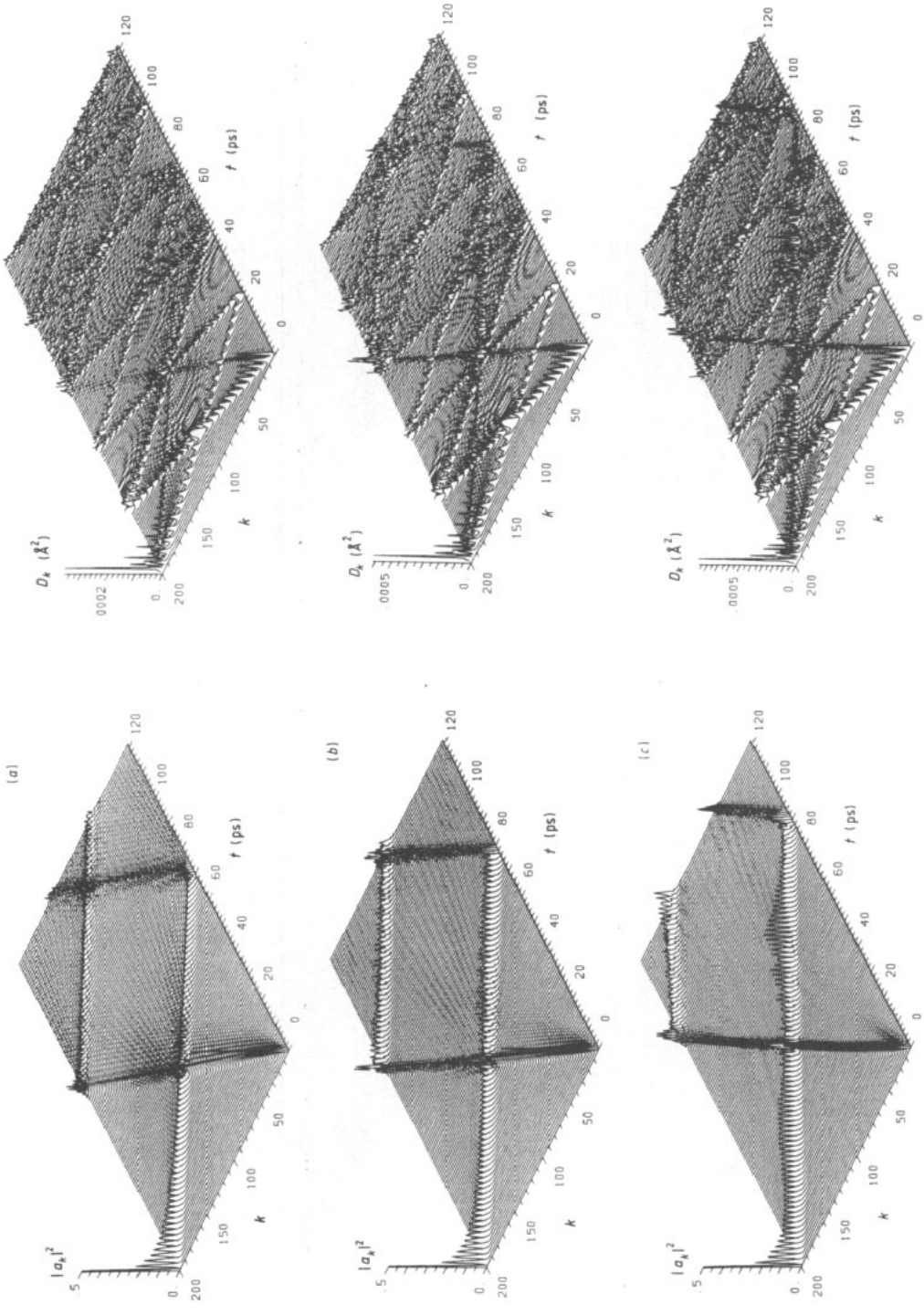
(a)
(b)
(c)
D_k (Å^2)
$|a_k|^2$
k
t (ps)

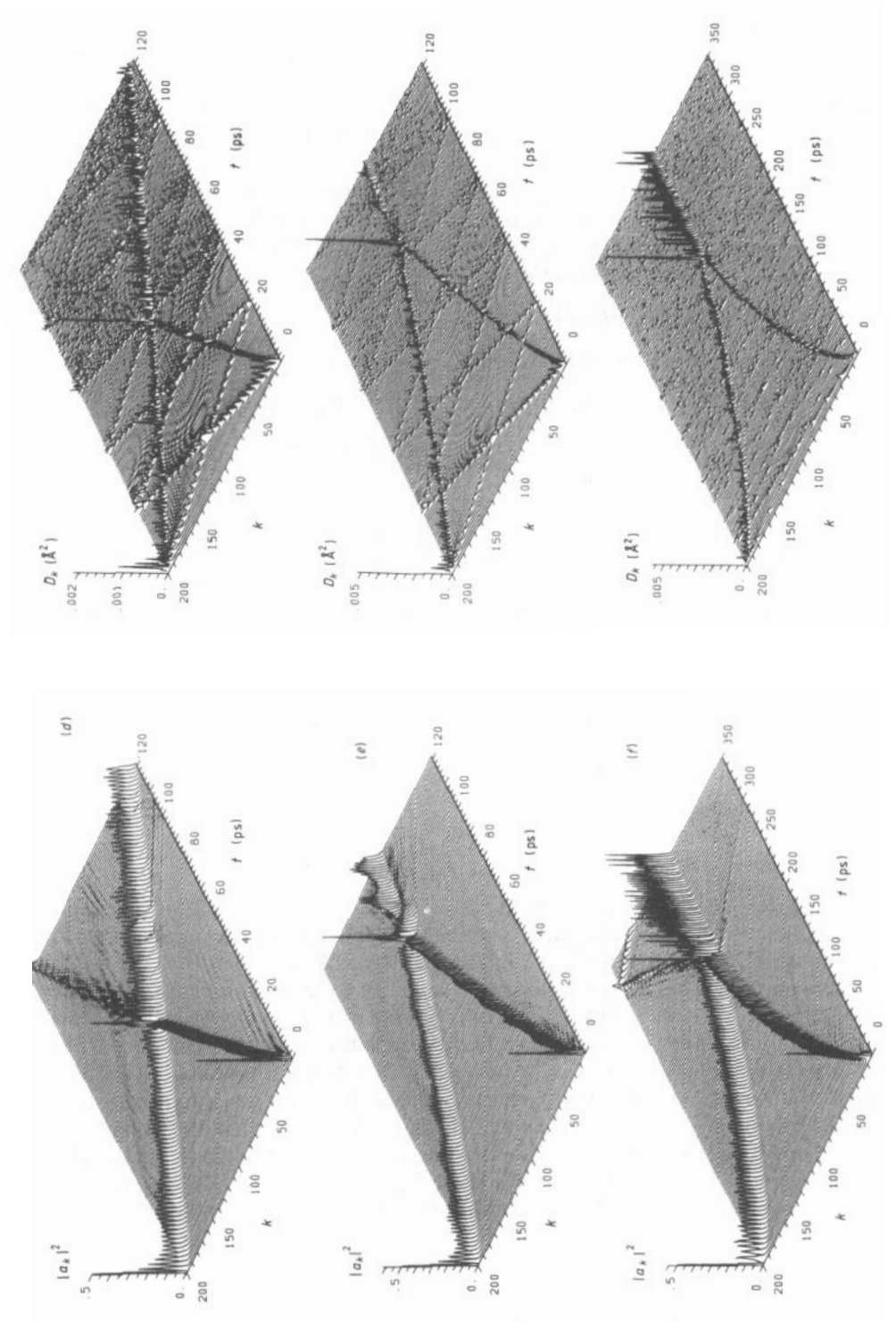

Figure 3. Time (t/ps) evolution of $|a_k(t)|^2$ and of $D_k = (q_k - q_{k-1})^2$ (Å^2) for soliton collisions after excitation at the terminal sites 2 and 199 as a function of X (the state contains two quanta): (*a*) $X = 30$ pN; (*b*) $X = 40$ pN; (*c*) $X = 50$ pN; (*d*) $X = 62$ pN; (*e*) $X = 70$ pN; (*f*) $X = 75$ pN.

from HM, it is shown [40] that even $q_n(t)$ is incorrect in the transportless case. However, optimized equations of motion for $|D_1\rangle$ have been derived [38, 39], which reproduce the exact solution in the $J = 0$ limit. Their numerical application to aperiodic chains is described.

Subsequently Brown *et al* [43] derived a theory based on an *ansatz* that is a special case of the $|D_1\rangle$ *ansatz* and contains $|D_2\rangle$ as one limiting case. They argue that in $|D_1\rangle$ overdressing might occur, and they introduce a dressing factor in their state, which is optimized variationally. Since $|D_2\rangle$ results can be mapped into the partial dressing theory [43], we decided to use the $|D_2\rangle$ *ansatz* state for our simulations. However, some numerical simulations using the $|\tilde{D}\rangle$ state *ansatz* are described below.

After a suitable gauge transformation

$$a_n' = a_n \exp(-iE_0 t/\hbar) \tag{4}$$

one obtains the equations of motion [17] as

$$i\hbar\dot{a}_n = E_n a_n - J(a_{n+1} + a_{n-1}) + X(q_n - q_{n-1})a_n \tag{5a}$$

$$\dot{p}_n = W(q_{n+1} - 2q_n + q_{n-1}) + QX(|a_{n+1}|^2 - |a_n|^2) \tag{5b}$$

$$\dot{q}_n = p_n/M. \tag{5c}$$

The complex equation (5*a*) was solved as a system of two coupled equations for the real and imaginary parts of a_n. The system of units eV for energy, Å for length and ps for time proved to be suitable for numerical solution of (5). We applied a Runge–Kutta method of fourth order [44, 45]. As we have shown [46] for two cases where equation (5) can be solved analytically, this algorithm works extremely well for equations of the type occurring here. We used a time step of $\tau = 0.005$ ps and a chain length of 200 units. In this case the total energy is typically conserved up to better than 0.01% and the norm to 0.4 ppm (parts per million). We used open chains with fixed ends as suggested in [46].

3. Results and discussion

3.1. Two-quantum dynamics

In our first series of computer experiments we used $a_n(0) = (\delta_{199,n} + \delta_{198,n})/\sqrt{2}$ as initial excitation, i.e. we put one vibrational quantum on each of the two sites close to the fixed chain end ($n = 200$), and varied the coupling constant X. If we put the two quanta initially on one site (199) the results do not change. In the case of one-quantum states, soliton formation is observed for $X > 40$ pN, and for $X > 80$ pN pinning of the soliton occurs [15, 30]. In figure 2(*a*) we show the time evolution of $|a_n(t)|^2$ for two-quantum states for different values of X. Obviously for $X \leqslant 20$ pN dispersive behaviour is obtained. However, already for $X = 30$ pN, in contrast to the one-quantum state, a soliton is formed that propagates with a velocity of $\simeq 0.93$ km s^{-1} through the chain. The solitary character of the wave is confirmed by the existence of the accompanying lattice distortion seen in figure 2(*b*), where we show $D_n = (q_n - q_{n-1})^2$. For $X = 40$ pN the velocity is reduced to 0.76 km s^{-1}, and starting with $X = 62$ pN the soliton is pinned. Thus in the two-quantum case the window for travelling solitons is shifted to smaller values of X.

If we put the two quanta initially on sites 100 and 101 in the middle of the chain, we obtain a similar behaviour as observed in the one-quantum case. Up to $X = 50$ pN the

excitation disperses, and from $X = 62$ pN a pinned soliton is formed. In the corresponding one-quantum case the behaviour is dispersive for $X = 62$ pN. Thus also here the threshold for soliton formation is at smaller X values than in the one-quantum case. (Figures corresponding to results described but not shown here can be obtained from the author upon request.)

One should note that an excitation in the middle of the chain must show a different time evolution than an excitation at the chain end owing to symmetry. From an excitation in the middle of the chain only three different time evolutions are possible by symmetry; (i) dispersive behaviour, (ii) two identical solitons travelling in opposite directions, or (iii) a pinned soliton, if the excitation is symmetric with respect to the centre of the chain as in our case. An excitation at the chain end can evolve without such symmetry restrictions. Thus the two cases are physically different. Since one may expect excitations at the chain ends [13, 16] to be more probable as a result of ATP hydrolysis, they seem to be more important. In our simulations we found no difference in the results if the terminal molecules are fixed as used here, or if they are allowed to move freely. In a survey of the (J, W, X) parameter space, we could find no case of travelling solitons for excitation in the centre of the chain, and only cases (i) and (iii) are realized.

Finally we studied soliton collisions. The initial excitation was $a_n(0) = (\delta_{2,n} + \delta_{199,n})/\sqrt{2}$. Thus at each chain end a one-quantum excitation starts to evolve, and therefore the threshold for soliton formation occurs around $X = 40$ pN as for one-quantum states. Note that, owing to the fact that we use an even number of units, the symmetry with respect to the centre of the chain does not hold completely because this centre is between sites 100 and 101, while our variables are only defined at the sites not between them. Thus the interaction of the solitons occurs not in the centre of the chain. Also the asymmetric interaction used might lead to symmetry breaking. For $X = 30$ pN (figure 3(*a*)) the behaviour is dispersive. At $X = 40$ pN (figure 3(*b*)) and $X = 50$ pN (figure 3(*c*)) the solitons pass each other without perturbation. At $X = 62$ pN (figure 3(*d*)) one of the two solitons propagates further with a larger amplitude while the other one is diminished and disperses after the collision. The two one-quantum solitons fuse partially. At $X = 70$ pN (figure 3(*e*)) the fusion of two one-quantum solitons to a pinned two-quantum soliton is almost complete, and at $X = 75$ pN (figure 3(*f*)) the fusion occurs fully, besides a small dispersing tail. A similar fusion effect of two solitons was reported earlier by Bolterauer [19]; however, he gave no parameter values in his paper. Obviously the formation of a soliton containing more than one quantum needs a finite time, and thus larger values of X (smaller soliton velocities) favour the fusion process in collisions.

3.2. *Diagonal disorder*

3.2.1. $|D_2\rangle$ dynamics. First we want to concentrate on the case where only the central site of the chain is disordered, i.e. $E_n = \Delta\delta_{n,100}$. In our first series of calculations a one-quantum soliton is started from the terminal site 199 and $X = 62$ pN. For $\Delta = -2$ meV the soliton is reflected from the impurity. In the lattice dynamics the distortion accompanying the soliton shows in all cases the same behaviour as $|a_n(t)|^2$ while the shock waves are not influenced by the impurity.

In case of $\Delta = -1$ meV the dynamics are more complicated. First of all the soliton is destroyed at the impurity site and equal fractions of the excitation are reflected and transmitted, but in a dispersive manner. A small part of the excitation is trapped at the impurity site. For $\Delta = -0.5$ meV the soliton is diminished in amplitude but able to pass the impurity. For Δ-values of the same absolute values but opposite signs the dynamics

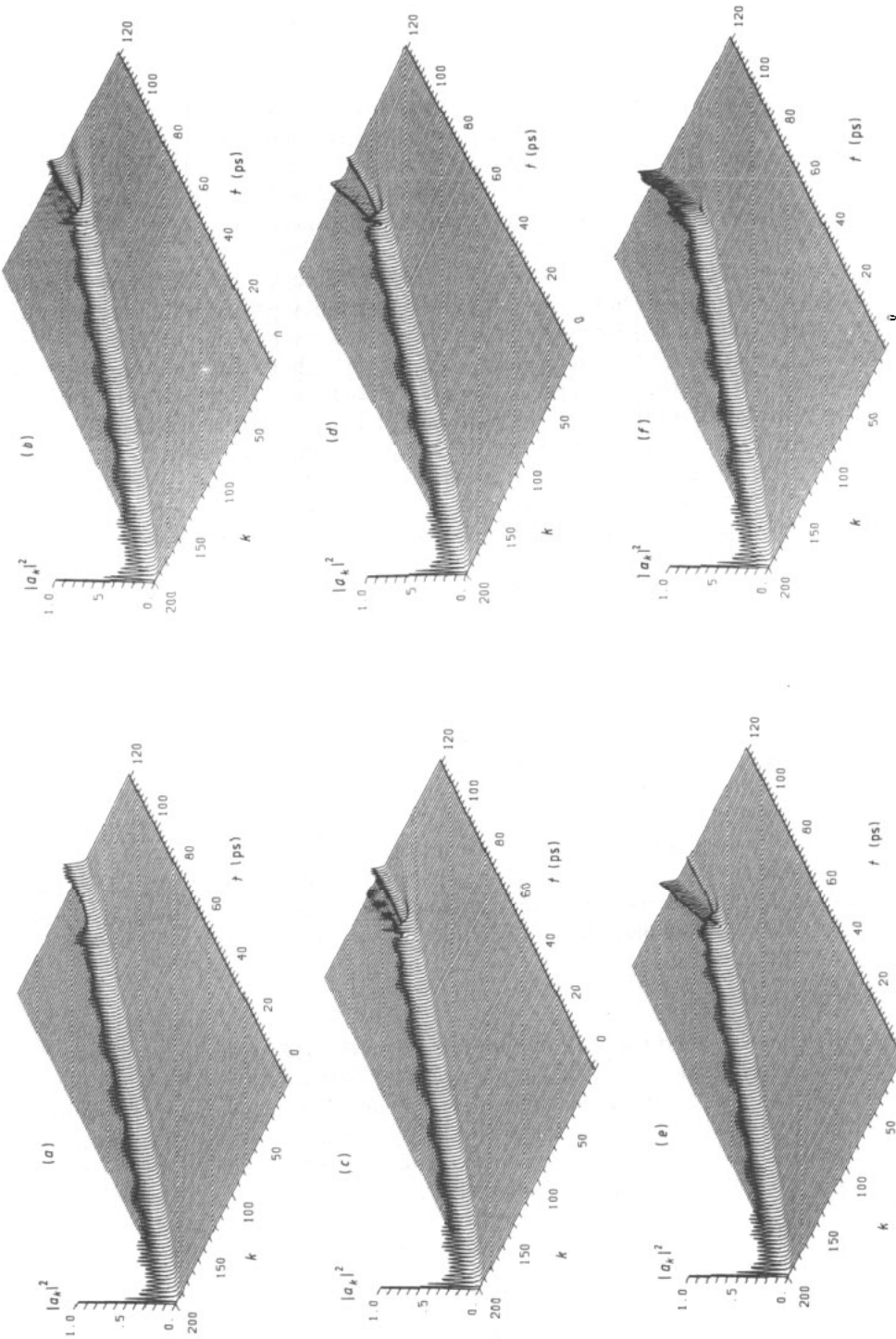

Figure 4. Time (t/ps) evolution of $|a_k(t)|^2$ for an isolated diagonal impurity ($E_n = \Delta\delta_{n,100}$) and a two-quantum solition for $X = 50\rho$N: (*a*) $\Delta = -0.2$ meV; (*b*) $\Delta = -0.4$ meV; (*c*) $\Delta = -0.6$ meV; (*d*) $\Delta = -0.8$ meV; (*e*) $\Delta = -1.0$ meV; (*f*) $\Delta = -2.0$ meV.

are the same as described above. Obviously the soliton is rather sensitive to a diagonal impurity. This might be due to the fact that via the terms

$$[E_n + X(q_n - q_{n-1})]a_n \tag{6}$$

in equation (5*a*) a diagonal impurity interferes directly with the non-linear coupling that makes the solitary behaviour of the wave possible. Since the coupling term is rather small (roughly of order 1–2 meV), a disorder $\Delta = \pm 0.5$ meV already interferes with the soliton.

From this argument one may expect that for $X = 50$ pN the soliton should be even more sensitive to the value of Δ. However, for smaller X the velocity of the soliton is larger and thus the interaction time of the soliton with the impurity is decreased. Both effects compete with each other, and we found that the soliton is slightly more stable in this case. For two-quantum states we used $X = 50$ pN since a two-quantum soliton is already pinned for $X = 62$ pN. Two-quantum solitons have a smaller velocity than their one-quantum counterparts. Thus we expect that they are more sensitive to the impurity. As figure 4 shows, this is indeed the case. Only for $\Delta = -0.2$ meV (figure 4(*a*)) is the soliton able to pass the impurity. For $\Delta = -0.4$ meV (figure 4(*b*)) considerable dispersion occurs. At $\Delta = -0.6$ meV (figure 4(*c*)) the dispersion is enhanced, and at $\Delta = -0.8$ meV (figure 4(*d*)) the soliton is more or less destroyed, while for $\Delta = -1$ meV (figure 4(*e*)) reflection starts. At $\Delta = -2$ meV (figure 4(*f*)) total reflection occurs.

If the coupling is lowered to $X = 40$ pN in the two-quantum case, the acceleration of the soliton dominates the dynamics. For $\Delta = -0.2$ and -0.5 meV the soliton is able to pass the impurity. Only at $\Delta = -1$ meV does dispersion occur and the soliton is destroyed, while for $\Delta = -2$ meV total reflection occurs. Thus two-quantum solitons for $X = 40$ pN behave very similarly to one-quantum solitons at $X = 62$ pN.

In the next step of our investigations we used a random sequence for E_n to simulate aperiodicity, where $E_n = \alpha_n \Delta$ and the α_n are random numbers with $|\alpha_n| \leqslant 1$. We performed simulations for $X = 62$ pN and one-quantum solitons. Our basic observation is that diagonal aperiodicity and temperature act strikingly similarly in the sense that the $|a_n|^2$ plots are very similar to that of [15] showing temperature effects. In both the $\Delta = 0.1$ meV case and the $T = 10$ K case in a perfect chain, the soliton passes along the chain with only small dispersion. In the case $\Delta = 0.2$ meV and $T = 40$ K from [15], the soliton disperses rather fast. For $\Delta = 1$ meV and $T = 300$ K, the excitation remains for a long time at the chain end and disperses very slowly into the chain. Finally, for $\Delta = 5$ meV pinning occurs, which resembles the $T = 300$ K case from [15] with larger coupling constant. If instead of equation (4) we use

$$a_n' = \bar{a}_n \exp[-(\mathrm{i}/\hbar)(E_n + E_0)t] \tag{7}$$

as transformation, we obtain instead of equation (5*a*) the following equation of motion:

$$\mathrm{i}\hbar\dot{\bar{a}}_n = -J[\bar{a}_{n+1} \exp(-(\mathrm{i}/\hbar)(E_{n+1} - E_n)t) + \bar{a}_{n-1} \exp((\mathrm{i}/\hbar)(E_n - E_{n-1})t)] + X(q_n - q_{n-1})\bar{a}_n. \tag{8}$$

Thus diagonal disorder in essence acts as a time- and site-dependent phase in the dipole–dipole coupling J. As shown in [21] the effects of temperature can be cast mathematically into the same form. This explains the similarity described above qualitatively. A reduction of the coupling to $X = 50$ pN results in no drastic changes. Again for $\Delta = 0.1$ meV a soliton is observed, while for $\Delta = 0.2$ meV it disperses, and for still larger disorder ($\Delta = 0.5$ meV) a tendency to pinning occurs. The two-quantum soliton ($X =$

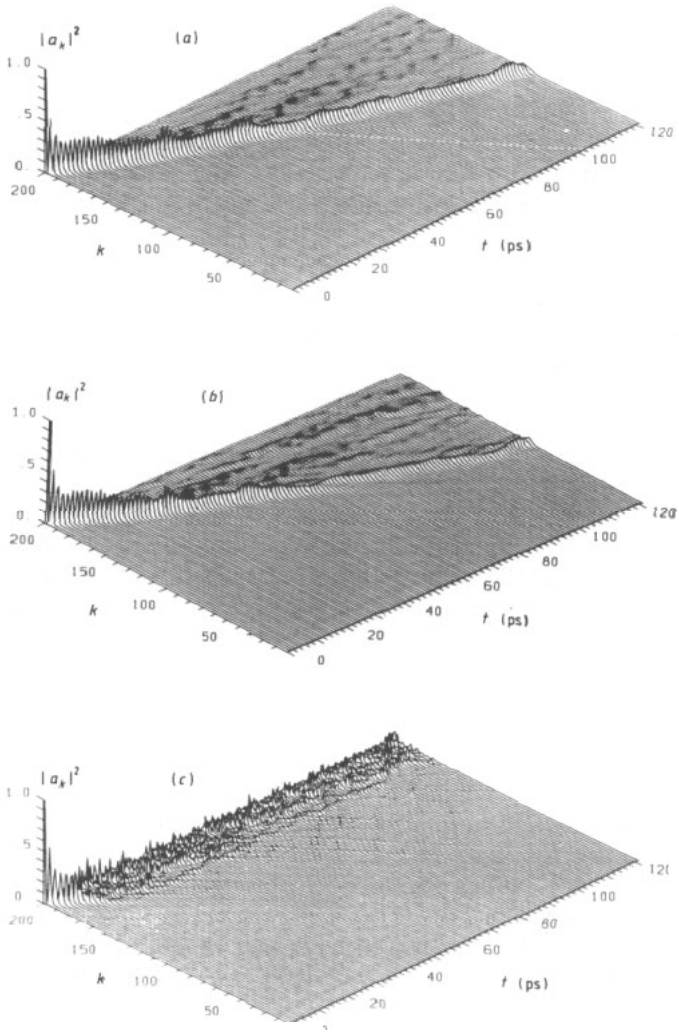

Figure 5. Time (t/ps) evolution of $|a_k(t)|^2$ for $X = 50$ pN, a two-quantum soliton and diagonal disorder ($E_n = \beta_n$; $|\beta_n| \leqslant 1$, β_n random): (*a*) $\Delta = 0.08$ meV; (*b*) $\Delta = 0.10$ meV; (*c*) $\Delta = 0.50$ meV.

50 pN) turns out to be more unstable against disorder, as figure 5 shows. For $\Delta = 0.08$ meV (figure 5(*a*)) we observe a soliton, while for $\Delta = 0.1$ meV (figure 5(*b*)) dispersion already occurs. At $\Delta = 0.5$ meV (figure 5(*c*)) again the tendency of pinning shows up. This reduced stability of the two-quantum soliton may again be attributed to its smaller velocity compared to that in the one-quantum case. Each impurity thus has more time to affect the soliton. Owing to the larger velocity in the case of smaller coupling, the stability of the two-quantum soliton increases if $X = 40$ pN. The soliton is stable from $\Delta = 0.08$ to 0.12 meV. At $\Delta = 0.14$ meV, fast dispersion is observed as expected.

3.2.2. Improved ansatz states. The $|D_1\rangle$ *ansatz* state as introduced by Davydov [22] reads as

$$|D_1\rangle = \sum_n \bar{a}_n(t)\hat{a}_n^+ |0\rangle_{ex} |\beta_n(t)\rangle \tag{9}$$

with

$$|\beta_n(t)\rangle = \exp[-\hat{S}_n(t)]|0\rangle_{ph} = \exp\left(-\sum_k (b_{nk}^* \hat{b}_k - b_{nk}\hat{b}_k^+)\right)|0\rangle_{ph}. \tag{10}$$

This *ansatz* allows dynamical phase mixing between phonons and excitons. Thus the quantum nature of the lattice is more pronounced than in the $|D_2\rangle$ state. Davydov's theory [22] results in equations of motion that do not reproduce the exact dynamics in the transportless case ($J = 0$). Recently [38, 39] optimized equations of motion have been derived that reproduce these exact dynamics. Including disorder, they read as

$$\begin{aligned} i\hbar\dot{a}_n = &\Big(E_n - \tfrac{1}{2} i\hbar \sum_k (\dot{b}_{nk} b_{nk}^* - \dot{b}_{nk}^* b_{nk}) \\ &+ \sum_k \hbar\omega_k [2B_{nk}\,\mathrm{Re}(b_{nk}) + |b_{nk}|^2]\Big) a_n \\ &- J_n D_{n,n+1} a_{n+1} - J_{n-1} D_{n,n-1} a_{n-1}. \end{aligned} \tag{11}$$

Here

$$\bar{a}_n = a_n \exp(-i E_0 t/\hbar) \tag{12}$$

and

$$D_{nn'} = \exp\left(-\tfrac{1}{2}\sum_k [|b_{nk} - b_{n'k}|^2 + 2\mathrm{Im}(b_{n'k}^* b_{nk})]\right). \tag{13}$$

Further

$$\begin{aligned} i\hbar\dot{b}_{nk} = &\hbar\omega_k(b_{nk} + B_{nk}) - J_n D_{n,n+1}(b_{n+1,k} - b_{nk}) a_{n+1}/a_n \\ &- J_{n-1} D_{n,n-1}(b_{n-1,k} - b_{nk}) a_{n-1}/a_n. \end{aligned} \tag{14}$$

To avoid numerical difficulties due to the denominators a_n in (14) we use the same initial conditions as in [39]. To check our program we have used the same initial and boundary conditions as in [39]. Our results for $X = 174$ pN are identical to those of figure 6 in [39]. Also the other figures of [39] could be reproduced.

We have used a chain of 50 units, obtained the normal modes **U** by numerical diagonalization of **V** (see appendix), and we did not populate the translational mode. We used $M = 114 m_p$, $W = 13$ N m^{-1}, $J = 0.967$ meV. For $X = 142$ pN the excitation is still dispersive. Only from $X \simeq 174$ pN is a travelling soliton observed, while between 200 and 300 pN pinning occurs in agreement with [39], although the boundary conditions are slightly different. We performed a survey of the parameter subspace $[W, X]$ for different values of J. These are $J = 0.6$, 0.967 and 1.4 meV. We found that travelling solitons exist only for $W < 50$ N m^{-1}, in contrast to $|D_2\rangle$ dynamics. Also the solitons occur for much larger values of X. The threshold value of X increases for increasing J as in $|D_2\rangle$ dynamics. One cannot expect soliton formation below $X \simeq 120$ pN within $|D_1\rangle$ dynamics. This value is well above all estimates of X for proteins ($\simeq$30–60 pN). However, there exists an experimental estimate for the X value of the N—H vibration as large as 339 pN [36].

For $N = 50$($X = 174$ pN) and a time step of 0.01 ps in our fourth-order Runge–Kutta method, within 12 ps the error in total energy is less than 0.011 meV, the norm error less

than 0.5×10^{-4}. We have calculated the influence of a diagonal impurity $E_n = \Delta\delta_{n,25}$ on a soliton ($X = 174$ pN). Up to $\Delta = 0.2$ meV the soliton is not much affected by the impurity, while from $\Delta = 0.3$ meV the trapped parts of the excitation are already quite large. Within a random sequence $E_n = \alpha_n\Delta$ ($|\alpha_n| \leq 1$, α_n random numbers), already at $\Delta = 0.15$ meV the soliton is slowly dispersive and full dispersion occurs from $\Delta = 0.20$ meV. Thus the sensitivity of the soliton against diagonal disorder is comparable to $|D_2\rangle$ models. In the case of a random distribution of masses, the natural variation of amino acid masses does not affect the soliton.

Brown *et al* [43] have introduced a modified *ansatz* state, which they call the $|\tilde{D}\rangle$ state. The $|\tilde{D}\rangle$ states are a subset of the generalized $|D_1\rangle$ states introduced by Davydov [22]. In this state, a fixed degree of phase mixing is incorporated:

$$|\tilde{D}\rangle = \sum_n a_n' \hat{a}_n'^{+} \exp\left(\sum_k (b_k' \hat{b}_k'^{+} - b_k'^{*} \hat{b}_k')\right)|0\rangle. \tag{15}$$

Here the operators are defined as

$$\hat{a}_n' = \hat{a}_n \exp\left(\delta \sum_k (B_{nk}\hat{b}_k^{+} - B_{nk}^{*}\hat{b}_k)\right) \tag{16}$$

$$\hat{b}_k' = \hat{b}_k + \delta \sum_n B_{nk}\hat{a}_n^{+}\hat{a}_n \tag{17}$$

where in an aperiodic chain (see appendix)

$$B_{nk} = \frac{X_n}{\omega_k}\frac{1}{(2\hbar\omega_k)^{1/2}}\left(\frac{U_{n+1,k}}{M_{n+1}^{1/2}} - \frac{U_{n,k}}{M_n^{1/2}}\right) \tag{18}$$

and δ is the dressing factor. In (18), ω_k are the eigenfrequencies of the decoupled lattice and $\mathbf{U}$ is the matrix containing its normal modes. The coefficients in the $|\tilde{D}\rangle$ state are related to those occurring in $|D_1\rangle$ by

$$a_n = a_n' \exp\left(-\mathrm{i}\delta \sum_k B_{nk}\,\mathrm{Im}(b_k')\right) \tag{19}$$

$$b_{nk} = -\delta B_{nk} + b_k'. \tag{20}$$

The dressing factor δ can be obtained by minimization of the averaged total energy [43]. Using equation (4.12) of [43] we have computed δ for $T = 0$ K in a periodic chain. For $0.8\ \text{meV} \leq J \leq 1.2$ meV, δ varies between 0.76 and 0.97, where δ decreases with increasing J. With increasing non-linearity, δ also increases; however, the larger W the smaller is the variation in δ, and the larger its value. Thus for increasing J and decreasing X and W, the $|\tilde{D}\rangle$ state approaches the $|D_2\rangle$ state ($\delta = 0$); while for decreasing J and increasing X and W, $|\tilde{D}\rangle$ approaches the small-polaron limit ($\delta = 1$). For $J = 0.967$ meV and $W = 10\ \text{N m}^{-1}$, δ varies by ≈ 0.15 in the range $0 \leq X \leq 200$ pN. For $X = 0$, $\delta \simeq 0.796$ is obtained, and for $X = 200$ pN, $\delta \simeq 0.944$. For $X \simeq 60$ pN, we obtain $\delta \simeq 0.81$, in agreement with Brown *et al* [43]. Thus for the usual values of the parameters, the $|\tilde{D}\rangle$ state is closer to the small-polaron limit than to the $|D_2\rangle$ state.

Brown *et al* [43] derived the equations of motion for the $|\tilde{D}\rangle$ state with the help of the time-dependent variational principle.

For numerical simulations a suitably small time step τ is introduced. During this time step (or half of it as in the Runge–Kutta method), the integrand is linearly interpolated. Thus at the time $l\tau$ we obtain

$$\begin{aligned} b'_k(l) &= A_k\, e^{-i\omega_k l\tau} + C_k(l) - i\omega_k\, e^{-i\omega_k l\tau} \sum_n B_{nk} D_{nk}(l) \\ A_k &= b'_k(0) - \delta \sum_n B_{nk} |a'_n(0)|^2 \\ C_k(l) &= \delta \sum_n B_{nk} |a'_n(l\tau)|^2 \\ D_{nk}(0) &= 0 \\ D_{nk}(l) &= D_{nk}(l-1) + \tfrac{1}{2}\tau[E_{nk}(l) + E_{nk}(l-1)] \\ E_{nk}(l) &= e^{i\omega_k l\tau}\, |a'_n(l\tau)|^2. \end{aligned} \tag{21}$$

For $T = 0$ K the initial phonon data are $b'_k(0) = 0$. After computation of $a_n(l\tau)$ and $b'_k(l\tau)$, the time derivative of $a'_n(l\tau)$ can be obtained by:

$$\begin{aligned} i\hbar \dot{a}'_n(l\tau) &= [E_0 + E_n - \delta(2-\delta)\varepsilon_n] a'_n(l\tau) - \bar{J}_n a'_{n+1}(l\tau) \\ &\quad - \bar{J}_{n-1} a'_{n-1}(l\tau) + 2 \sum_k \hbar\omega_k B_{nk}\, \mathrm{Re}(b'_k(l\tau)) a'_n(l\tau) \\ &\quad + 2\delta(1-\delta) \sum_{m,k} \hbar\omega_k B_{nk} B_{mk} |a'_m(l\tau)|^2 a'_n(l\tau). \end{aligned} \tag{22}$$

Here E_n represents the disorder of the on-site oscillator energy ($E_0 + E_n$), ε_n is given by

$$\varepsilon_n = \sum_k B_{nk}^2 \hbar\omega_k \tag{23}$$

which is the small-polaron binding energy [43], and the scaled oscillator coupling is

$$\bar{J}_n = J_n \exp\left(-\tfrac{1}{2}\delta^2 \sum_k (B_{nk} - B_{n+1,k})^2 \right). \tag{24}$$

From $\dot{a}'_n(l\tau)$, $a'_n((l+1)\tau)$ can be computed. In practice, a gauge transformation is performed

$$a'_n = a''_n \exp(-i\, E_0 t/\hbar) \tag{25}$$

which removes the term containing E_0 and thus the rapidly oscillating part of a'_n.

Typically we used $\tau = 0.01$ ps for our simulations within a Runge–Kutta method correct up to fourth order [21, 45]. In this case ($M = 114m_p$, $W = 13$ N m^{-1}, $J = 0.967$ meV, $X = 180$ pN) for a periodic chain of 50 units, within 12 ps the error in total energy is less than 0.015 meV ($\simeq 0.004\%\ E_t$) and the norm is conserved to better than 0.36×10^{-4}. Here $\delta = 0.9016$. The translational mode was kept unpopulated. Our calculations have been performed with the same parameters as for $|D_1\rangle$ ($M = 114m_p$, $W = 13$ N m^{-1}, $J = 0.967$ meV, $X = 60$, 100, 140, 180, 220, 260 pN). First of all, in contrast to $|D_2\rangle$ or $|D_1\rangle$ dynamics, no real moving soliton shows up. Only from $X = 180$ pN can one speak of a slowly dispersive solitary wave. For $X = 260$ pN a pinned soliton is observed. For the $|\tilde{D}\rangle$ state the parameter space that allows soliton formation is very small and at rather large values of X. Thus if the $|\tilde{D}\rangle$ state is a better approximation

to the exact solution than $|D_2\rangle$ or $|D_1\rangle$, one has to conclude that the Davydov soliton cannot exist in proteins at $T = 0$ K. However, the $|\tilde{D}\rangle$ states and the new equations of motion for $|D_1\rangle$ are both derived with the time-dependent variational principle. Therefore, the $|D_1\rangle$ dynamics should be a better approximation to the exact solution than the $|\tilde{D}\rangle$ states.

We have also calculated here soliton dynamics in disordered chains up to 70 ps in the case $W = 13$ N m^{-1}, $M = 114m_p$, $J = 0.967$ meV and $X = 240$ N. The time step was chosen to be $\tau = 5$ fs. In a typical simulation the energy error was less than 0.05 meV and the norm error less than 0.3×10^{-3}. In the periodic chain in the case of $|\tilde{D}\rangle$ dynamics we deal only with slowly dispersive solitary waves rather than with travelling solitons also for $X = 240$ pN. For an isolated impurity $E_n = \Delta\delta_{n,25}$ we find that for $\Delta = 0.1$ meV the wave is able to pass the impurity, while it is trapped for $\Delta = 0.2$ meV. In the case of random sequences $E_n = \alpha_n\Delta$ ($|\alpha_n| \leq 1$, random) for $\Delta = 0.05$ meV besides a considerable disturbance the wave is still travelling, while for $\Delta = 0.10$ meV it is destroyed. Finally, in the case of a random sequence of masses (between glycine and tryptophan) the excitation remains trapped for roughly 20 ps and disperses later on. Thus solitary waves in the $|\tilde{D}\rangle$ model are far more sensitive to disorder than solitons in $|D_2\rangle$ or $|D_1\rangle$ theory.

4. Conclusions

We studied two-quantum dynamics in the Davydov model system. In perfect chains we observed that the window for formation of propagating solitons is shifted to smaller values of the coupling X compared with the one-quantum case. In the case of soliton collisions we observe fusion of two one-quantum solitons to one pinned two-quantum soliton for high values of X ($X \geq 62$ pN). As Bolterauer [19] pointed out, this may indicate instability of two-quantum solitons with respect to one-quantum solitons, because of time reversal symmetry.

Both types of solitons are extremely unstable to diagonal disorder. This is due to the fact that diagonal disorder interferes directly with the coupling term to the lattice phonons in the equations of motion. Here, owing to their smaller velocities, two-quantum solitons are more sensitive to disorder than one-quantum solitons. Since the mathematical effects of diagonal disorder and temperature [21] can be cast into the same form, the results are quite similar: increasing disorder corresponds to increasing temperature; however, diagonal disorder effects are more dramatic than temperature effects.

In the case of the $|D_1\rangle$ *ansatz* state, which allows the quantum nature of the lattice to play a greater role, we found that solitons appear at much larger values of the coupling constant X than all estimates of X for proteins. In the case of the partial dressing state $|\tilde{D}\rangle$, no travelling solitons occur between $X = 0$ and 300 pN. However, $|D_1\rangle$ should be superior to $|\tilde{D}\rangle$ since it is more flexible, and the equations of motion for both states can be derived by the time-dependent variational principle. The sensitivity of solitons and solitary waves against diagonal disorder is comparable in all three *ansatz* states.

The results reported here for soliton–impurity interactions agree qualitatively with results published on the same problem in different systems. In one paper the case of *trans*-polyacetylene with site and bond impurities using the Hückel-type Su–Schrieffer–Heeger Hamiltonian was studied [47]. In another work the dynamics of point masses interacting via cubic, quartic and Morse potentials were investigated [48]. In both

studies, reflection, trapping and transmission together with partial reflection of solitons was observed depending on the strength of the impurity and the non-linearity. Qualitatively the same effects were observed here for Davydov solitons. However, quantitative comparisons cannot be made owing to the differences in the physical systems studied.

Acknowledgments

The financial support of the 'Deutsche Forschungsgemeinschaft' (Project No. Ot 51/6–2) and the 'Fonds der Chemischen Industrie' is gratefully acknowledged.

Appendix. Inclusion of disorder

We start with the classical equations of motion for a chain of N harmonically coupled point masses (M_n):

$$\mathbf{M}\ddot{\boldsymbol{q}} = -\mathbf{W}\boldsymbol{q} \qquad M_{nm} = M_n\delta_{nm}$$

$$W_{nm} = [W_n(1-\delta_{nN}) + W_{n-1}(1-\delta_{n1})]\delta_{nm} - W_n(1-\delta_{nN})\delta_{m,n+1} - W_{n-1}(1-\delta_{n1})\delta_{m,n-1} \tag{A1}$$

where q_n is the displacement of unit n and W_n is the force constant between units n and $n+1$. Here $p_n = M_n\dot{q}_n$ are the momenta of the units. Using the transformation

$$\mathbf{V} = \mathbf{M}^{-1/2}\mathbf{W}\mathbf{M}^{-1/2} \qquad \boldsymbol{d} = \mathbf{M}^{1/2}\boldsymbol{q} \qquad \boldsymbol{p} = \mathbf{M}^{1/2}\dot{\boldsymbol{d}} \tag{A2}$$

we obtain

$$\ddot{\boldsymbol{d}} = -\mathbf{V}\boldsymbol{d}. \tag{A3}$$

The Hamiltonian function is transformed as

$$2H_{\mathrm{ph}} = \boldsymbol{p}^+\mathbf{M}^{-1}\boldsymbol{p} + \boldsymbol{q}^+\mathbf{W}\boldsymbol{q} = \dot{\boldsymbol{d}}^+\dot{\boldsymbol{d}} + \boldsymbol{d}^+\mathbf{V}\boldsymbol{d}. \tag{A4}$$

Equation (A3) can be further simplified by transformation to normal modes $\boldsymbol{U}_k$ with $\boldsymbol{d}(t) = \Sigma_k \boldsymbol{U}_k(\mathbf{U}^+\boldsymbol{d}(0))_k \exp(\mathrm{i}\omega_k t)$ such that

$$\mathbf{U}^+\mathbf{V}\mathbf{U} = \boldsymbol{\omega}^2 \qquad \omega_{kl} = \omega_k\delta_{kl}. \tag{A5}$$

$\mathbf{V}$ can be numerically diagonalized and $\mathbf{U}$ chosen to be real. With $\boldsymbol{b} = \mathbf{U}^+\boldsymbol{d}$ we obtain

$$2H_{\mathrm{ph}} = \dot{\boldsymbol{b}}^+\dot{\boldsymbol{b}} + \boldsymbol{b}^+\boldsymbol{\omega}^2\boldsymbol{b} \tag{A6}$$

and with $\boldsymbol{b} = \hbar^{1/2}\boldsymbol{\omega}^{-1/2}\boldsymbol{a}$, $\boldsymbol{c} = \boldsymbol{\omega}^{-1}\dot{\boldsymbol{a}}$

$$2H_{\mathrm{ph}} = \sum_k \hbar\omega_k(c_k^*c_k + a_k^*a_k). \tag{A7}$$

Now creation ($\hat{b}_k^+$) and annihilation ($\hat{b}_k$) operators are introduced in the usual way to obtain the phonon part of the Hamiltonian operator

$$a_k \to (1/\sqrt{2})(\hat{b}_k + \hat{b}_k^+) \qquad c_k \to -(\mathrm{i}/\sqrt{2})(\hat{b}_k - \hat{b}_k^+) \tag{A8}$$

which leads to

$$\hat{H}_{\mathrm{ph}} = \sum_k \hbar\omega_k(\hat{b}_k^+\hat{b}_k + \tfrac{1}{2}). \tag{A9}$$

Thus finally

$$\begin{aligned}\hat{q}_n &= \sum_k [\hbar/(2M_n\omega_k)]^{1/2} U_{nk}(\hat{b}_k + \hat{b}_k^+)\\ \hat{p}_n &= -\mathrm{i}\sum_k [\hbar M_n\omega_k/2]^{1/2} U_{nk}(\hat{b}_k - \hat{b}_k^+).\end{aligned} \tag{A10}$$

Introducing (A10) into the full Hamiltonian, we obtain

$$\begin{aligned}\hat{H} = &\sum_n (E_0 + E_n)\hat{a}_n^+\hat{a}_n - \sum_n J_n(\hat{a}_n^+\hat{a}_{n+1} + \hat{a}_{n+1}^+\hat{a}_n)\\ &+ \sum_k \hbar\omega_k(\hat{b}_k^+\hat{b}_k + \tfrac{1}{2}) + \sum_{n,k} \hbar\omega_k B_{nk}(\hat{b}_k + \hat{b}_k^+)\hat{a}_n^+\hat{a}_n\end{aligned} \tag{A11}$$

with

$$B_{nk} = \frac{X_n}{\omega_k}\left(\frac{1}{2\hbar\omega_k}\right)^{1/2}\left(\frac{U_{n+1,k}}{M_{n+1}^{1/2}} - \frac{U_{nk}}{M_n^{1/2}}\right). \tag{A12}$$

References

[1] Fermi E, Pasta J R and Ulam S M 1955 *Los Alamos Report* LA–1940
[2] Scott-Russel J 1844 *Proc. R. Soc. Edin.* 319
[3] Mikeska H J 1978 *J. Phys. C: Solid State Phys.* **11** L29
[4] Maki K 1980 *J. Low Temp. Phys.* **41** 327
[5] Wahlstrand K J 1985 *J. Chem. Phys.* **82** 5247
Wahlstrand K J and Woylness P G 1976 *J. Chem. Phys.* **82** 3392
[6] Aubry S 1976 *J. Chem. Phys.* **64** 3392
[7] Collins M A, Blumen A, Curtis J F and Ross J 1979 *Phys. Rev.* B **19** 3630
[8] Krumhansl J A and Alexander D M 1983 *Structure and Dynamics: Nucleic Acids and Proteins* ed E Clementi and R H Sarma (New York: Adenine) p 61
[9] Ladik J and Cizek J 1984 *Int. J. Quantum Chem.* **26** 955
Ladik J 1985 *Molecular Basis of Cancer* Part A, ed R Rein (New York: Alan R Liss) p 343
Hofmann D, Förner W and Ladik J 1988 *Phys. Rev.* A **37** 4429
Förner W 1988 *Phys. Rev.* A **38** 939; 1989 *Phys. Rev.* A **40** 6435
Förner W, Otto P, Ladik J and Martino F 1989 *Phys. Rev.* A **40** 6457
Hofmann D, Förner W and Ladik J 1990 *J. Phys.: Condens. Matter* **2** 4081
[10] Takeno S and Homma S 1983 *Prog. Theor. Phys.* **70** 308; 1984 *Prog. Theor. Phys.* **72** 679; 1987 *Prog. Theor. Phys.* **77** 548
[11] Su W P, Schrieffer J R and Heeger A J 1979 *Phys. Rev. Lett.* **42** 1698
Su W P 1980 *Solid State Commun.* **35** 899
Su W P, Schrieffer J R and Heeger A J 1980 *Phys. Rev.* B **22** 2099
Su W P and Schrieffer J R 1980 *Proc. Natl. Acad. Sci. USA* **77** 5626
Guinea F 1984 *Phys. Rev.* B **30** 1884
Bishop A R, Campbell D K, Lomdahl R P, Horovitz B and Phillpot S R 1984 *Phys. Rev. Lett.* **52** 671
Förner W, Seel M and Ladik J 1986 *Solid State Commun.* **57** 463; 1986 *J. Chem. Phys.* **84** 5910
Godzik M, Seel M, Förner W and Ladik J 1987 *Solid State Commun.* **60** 609
Liegener C-M, Förner W and Ladik J 1987 *Solid State Commun.* **61** 203
Phillpot S R, Beariswyl D, Bishop A R and Lomdahl P S 1987 *Phys. Rev.* B **35** 7533
Kivelson S and Heim D E 1982 *Phys. Rev.* B **26** 4278

Heeger A J and Schrieffer J R 1983 *Solid State Commun.* **48** 207
Soos Z and Ramasesha S 1983 *Phys. Rev. Lett.* **51** 2374
Sasai M and Fukutome H 1984 *Synth. Met.* **9** 295
Su W P 1986 *Phys. Rev.* B **34** 2988
Kivelson S and Wei-Kang Wu 1986 *Phys. Rev.* B **34** 5423
Wang C-L and Martino F 1986 *Phys. Rev.* B **34** 5540
Förner W, Wang C-L, Martino F and Ladik J 1988 *Phys. Rev.* B **37** 4567
Förner W 1987 *Solid State Commun.* **63** 941
Markus R, Förner W and Ladik J 1988 *Solid State Commun.* **68** 135
Orendi H, Förner W and Ladik J 1988 *Chem. Phys. Lett.* **150** 113
[12] Szent-Györgyi A 1941 *Nature* **148** 157; 1941 *Science* **93** 609
Bakhshi A K, Otto P, Ladik J and Seel M 1986 *Chem. Phys.* **20** 683
[13] Davydov A S and Kislukha N I 1973 *Phys. Status Solidi* b **59** 465
Davydov A S 1979 *Phys. Scr.* **20** 387; 1982 *Sov. Phys.–Usp.* **25** 898; 1982 *Biology and Quantum Mechanics* (Oxford: Pergamon)
[14] Careri G, Buontempo U, Galuzzi F, Scott A C, Gratton E and Shyamsunder E 1984 *Phys. Rev.* B **30** 4689
Eilbeck J C, Lomdahl P S and Scott A C 1984 *Phys. Rev.* B **30** 4703
[15] Förner W and Ladik J 1991 *Davydov's Soliton Revisited: Self Trapping of Vibrational Energy in Proteins (Nato ASI Series B, 243)* ed P L Christiansen and A C Scott (New York: Plenum)
[16] Scott A C 1982 *Phys. Rev.* A **26** 578
[17] Kerr W C and Lomdahl P S 1991 *Davydov's Soliton Revisited: Self Trapping of Vibrational Energy in Proteins (Nato ASI Series B, 243)* ed P L Christiansen and A C Scott (New York: Plenum)
[18] Lomdahl P S and Kerr W C 1991 *Davydov's Soliton Revisited: Self Trapping of Vibrational Energy in Proteins (Nato ASI Series B, 243)* ed P L Christiansen and A C Scott (New York: Plenum)
[19] Bolterauer H 1986 *Structure, Coherence and Chaos* (*Proc. MIDIT 1986 Workshop*) (Manchester: Manchester University Press)
[20] Motschmann H, Förner W and Ladik J 1989 *J. Phys.: Condens. Matter* **1** 5083
[21] Förner W 1991 *J Phys.: Condens Matter* **3** at press
[22] Davydov A S 1980 *Zh. Eksp. Teor. Fiz.* **78** 789; 1980 *Sov. Phys.–JETP* **51** 397
[23] Halding J and Lomdahl P S 1987 *Phys. Lett.* A **124** 37
[24] Lomdahl P S and Kerr W C 1985 *Phys. Rev. Lett.* **55** 1235
[25] Lawrence A F, McDaniel J C, Chang D B, Pierce B M and Birge R R 1986 *Phys. Rev.* A **33** 1188
[26] Bolterauer H 1986 *Structure, Coherence and Chaos* (*Proc. MIDIT 1986 Workshop*) (Manchester: Manchester University Press)
[27] Cruzeiro L, Halding J, Christiansen P L, Skovgaard O and Scott A C 1988 *Phys. Rev.* A **37** 880
[28] Cottingham J P and Schweitzer J W 1989 *Phys. Rev. Lett.* **62** 1792
[29] Wang X, Brown D W and Lindenberg K 1989 *Phys. Rev. Lett.* **62** 1796
[30] Scott A C 1982 *Phys. Rev.* A **26** 578; 1983 *Structure and Dynamics: Nucleic Acids and Proteins* ed E Clementi and R H Sarma (New York: Adenine) p 389; 1984 *Phys. Scr.* **29** 279
MacNeil L and Scott A C 1984 *Phys. Scr.* **29** 284
Scott A C 1985 *Phil. Trans. R. Soc. Lond.* A **315** 423
[31] Ziman J M 1969 *Elements of Advanced Quantum Theory* (Cambridge: Cambridge University Press)
[32] Nevskaya N A and Chirgadze Y N 1976 *Biopolymers* **15** 637
[33] Itoh K and Shimanouchi T 1972 *J. Mol. Spectrosc.* **42** 86
[34] Novak A 1974 *Structure and Bonding* vol 18 (Berlin: Springer)
[35] Kuprievich V A and Klymenko V E 1977 *Mol. Phys.* **34** 1287
[36] Bierce B M 1991 *Davydov's Soliton Revisited: Self Trapping of Vibrational Energy in Proteins (Nato ASI Series B, 243)* ed P L Christiansen and A C Scott (New York: Plenum)
[37] Kerr W C and Lomdahl P S 1987 *Phys. Rev.* B **35** 3629
[38] Skrinjar M J, Kapor D V and Stojanovic S D 1988 *Phys. Rev.* A **38** 6402; 1989 *Phys. Rev.* B **40** 1984
[39] Muhtly B and Shaw P B 1988 *Phys. Rev.* B **38** 3075
[40] Brown D W, Lindenberg K and West B J 1986 *Phys. Rev.* A **33** 4104
Brown D W, West B J and Lindenberg K 1986 *Phys. Rev.* A **33** 4110
Brown D W 1988 *Phys. Rev.* A **37** 5010
[41] Brown D W, Lindenberg K and West B J 1987 *Phys. Rev.* B **35** 6169
[42] Brown D W, Lindenberg K and West B J 1988 *Phys. Rev.* B **37** 2946

[43] Brown D W and Ivic Z 1989 *Phys. Rev.* B **40** 9876
[44] Stiefel J 1965 *Einführung in die numerische Mathematik* (Stuttgart: Teubner)
[45] Abramowitz M and Stegun I A 1965 *Handbook of Mathematical Functions* (New York: Dover) eq. (25.2.20), p 897
[46] Förner W 1991 *J. Comput. Chem.* submitted
[47] Phillpot S R, Baeriswyl D, Bishop A R and Lomdahl P S 1987 *Phys. Rev.* B **35** 7533
[48] Li Q, Pnevmatikos S, Economou E N and Soukoulis C M 1988 *Phys. Rev.* B **37** 3534